Search for an Excess of Electron Neutrino Interactions in MicroBooNE Using Multiple Final-State Topologies

P. Abratenko,³³ R. An,¹⁴ J. Anthony,⁴ L. Arellano,¹⁸ J. Asaadi,³² A. Ashkenazi,³⁰ S. Balasubramanian,¹¹ B. Baller,¹¹ C. Barnes,²⁰ G. Barr,²³ V. Basque,¹⁸ L. Bathe-Peters,¹³ O. Benevides Rodrigues,²⁹ S. Berkman,¹¹ A. Bhanderi,¹⁸ A. Bhat,²⁹ M. Bishai,² A. Blake,¹⁶ T. Bolton,¹⁵ J. Y. Book,¹³ L. Camilleri,⁹ D. Caratelli,¹¹ I. Caro Terrazas,⁸ F. Cavanna,¹¹ G. Cerati,¹¹ Y. Chen,¹ D. Cianci,⁹ G. H. Collin,¹⁹ J. M. Conrad,¹⁹ M. Convery,²⁶ L. Cooper-Troendle,³⁶ J. I. Crespo-Anadón,⁵ M. Del Tutto,¹¹ S. R. Dennis,⁴ P. Detje,⁴ A. Devitt,¹⁶ R. Diurba,¹⁸ R. Dorrill,¹⁴ K. Duffy,¹¹ S. Dytman,²⁴ B. Eberly,²⁸ A. Ereditato,¹ L. Escudero Sanchez,⁴ J. J. Evans,¹⁸ R. Fine,¹⁷ G. A. Fiorentini Aguirre,²⁷ R. S. Fitzpatrick,²⁰ B. T. Fleming,³⁶ N. Foppiani,¹³ D. Franco,³⁶ A. P. Furmanski,²¹ D. Garcia-Gamez,¹² S. Gardiner,¹¹ G. Ge,⁹ V. Genty,⁹ S. Gollapinni,^{31,17} O. Goodwin,¹⁸ E. Gramellini,¹¹ P. Green,¹⁸ H. Greenlee,¹¹ W. Gu,² R. Guenette,¹³ P. Guzowski,¹⁸ L. Hagaman,³⁶ O. Hen,¹⁹ C. Hilgenberg,²¹ G. A. Horton-Smith,¹⁵ A. Hourlier,¹⁹ R. Itay,²⁶ C. James,¹¹ X. Ji,² L. Jiang,³⁴ J. H. Jo,³⁶ R. A. Johnson,⁷ Y.-J. Jwa,⁹ D. Kaleko,⁹ D. Kalra,⁹ N. Kamp,¹⁹ N. Kaneshige,³ G. Karagiorgi,⁹ W. Ketchum,¹¹ M. Kirby,¹¹ T. Kobilarcik,¹¹ I. Kreslo,¹ R. LaZur,⁸ I. Lepetic,²⁵ K. Li,³⁶ Y. Li,² K. Lin,¹⁷ A. Lister,¹⁶ B. R. Littlejohn,¹⁴ W. C. Louis,¹⁷ X. Luo,³ K. Manivannan,²⁹ C. Mariani,³⁴ D. Marsden,¹⁸ J. Marshall,³⁵ D. A. Martinez Caicedo,²⁷ T. Mohayai,¹¹ J. Moon,¹⁹ M. Moconey,⁸ A. F. Moor,⁴ C. D. Moore,¹¹ L. Mora Lepin,¹⁸ J. Mousseau,²⁰ M. Murphy,³⁴ T. Mohayai,¹¹ J. Moon,¹⁹ M. Moconey,⁸ A. F. Moor,⁴ C. D. Moore,¹¹ L. Nora Lepin,¹⁸ J. Mousseau,²⁰ M. Murphy,³⁴ D. Naples,²⁴ A. Nayrer-Agasson,¹⁸ M. Nebot-Guinot,¹⁰ R. K. Neely,¹⁵ D. A. Newmark,¹⁷ J. Nowak,¹⁶ M. Nunes,²⁹ O. Palamara,¹¹ V. Paolone,²⁴ A. Papadopoulou,¹⁹

(MicroBooNE Collaboration)*

¹Universität Bern, Bern CH-3012, Switzerland ²Brookhaven National Laboratory (BNL), Upton, New York 11973, USA ³University of California, Santa Barbara, California 93106, USA ⁴University of Cambridge, Cambridge CB3 0HE, United Kingdom ⁵Centro de Investigaciones Energéticas, Medioambientales y Tecnológicas (CIEMAT), Madrid E-28040, Spain ⁶University of Chicago, Chicago, Illinois 60637, USA ⁷University of Cincinnati, Cincinnati, Ohio 45221, USA ⁸Colorado State University, Fort Collins, Colorado 80523, USA ⁹Columbia University, New York, New York 10027, USA ¹⁰University of Edinburgh, Edinburgh EH9 3FD, United Kingdom ¹¹Fermi National Accelerator Laboratory (FNAL), Batavia, Illinois 60510, USA ¹²Universidad de Granada, Granada E-18071, Spain ¹³Harvard University, Cambridge, Massachusetts 02138, USA ¹⁴Illinois Institute of Technology (IIT), Chicago, Illinois 60616, USA ⁵Kansas State University (KSU), Manhattan, Kansas 66506, USA ¹⁶Lancaster University, Lancaster LA1 4YW, United Kingdom ¹⁷Los Alamos National Laboratory (LANL), Los Alamos, New Mexico 87545, USA ¹⁸The University of Manchester, Manchester M13 9PL, United Kingdom ¹⁹Massachusetts Institute of Technology (MIT), Cambridge, Massachusetts 02139, USA ²⁰University of Michigan, Ann Arbor, Michigan 48109, USA ²¹University of Minnesota, Minneapolis, Minnesota 55455, USA ²²New Mexico State University (NMSU), Las Cruces, New Mexico 88003, USA ²³University of Oxford, Oxford OX1 3RH, United Kingdom

²⁴University of Pittsburgh, Pittsburgh, Pennsylvania 15260, USA
 ²⁵Rutgers University, Piscataway, New Jersey 08854, USA
 ²⁶SLAC National Accelerator Laboratory, Menlo Park, California 94025, USA
 ²⁷South Dakota School of Mines and Technology (SDSMT), Rapid City, South Dakota 57701, USA
 ²⁸University of Southern Maine, Portland, Maine 04104, USA
 ²⁹Syracuse University, Syracuse, New York 13244, USA
 ³⁰Tel Aviv University, Tel Aviv, Israel, 69978
 ³¹University of Tennessee, Knoxville, Tennessee 37996, USA
 ³²University of Texas, Arlington, Texas 76019, USA
 ³³Tufts University, Medford, Massachusetts 02155, USA
 ³⁴Center for Neutrino Physics, Virginia Tech, Blacksburg, Virginia 24061, USA
 ³⁵University of Warwick, Coventry CV4 7AL, United Kingdom
 ³⁶Wright Laboratory, Department of Physics, Yale University, New Haven, Connecticut 06520, USA

(Received 29 October 2021; accepted 13 April 2022; published 13 June 2022)

We present a measurement of ν_e interactions from the Fermilab Booster Neutrino Beam using the MicroBooNE liquid argon time projection chamber to address the nature of the excess of low energy interactions observed by the MiniBooNE Collaboration. Three independent ν_e searches are performed across multiple single electron final states, including an exclusive search for two-body scattering events with a single proton, a semi-inclusive search for pionless events, and a fully inclusive search for events containing all hadronic final states. With differing signal topologies, statistics, backgrounds, reconstruction algorithms, and analysis approaches, the results are found to be either consistent with or modestly lower than the nominal ν_e rate expectations from the Booster Neutrino Beam and no excess of ν_e events is observed.

DOI: 10.1103/PhysRevLett.128.241801

MicroBooNE is the first liquid argon time projection chamber (LArTPC) to acquire high statistics samples of neutrino interactions on argon. Using this unique dataset, MicroBooNE has pioneered a large body of results on neutrino interactions [1–7], astrophysical [8,9], and beyond the standard model physics [10,11], neutrino event reconstruction [12–23], and detector properties [24–33]. Here, we report the first measurement of electron neutrinos produced in the Fermilab Booster Neutrino Beamline (BNB) using the MicroBooNE detector. This multipronged search is aimed at investigating the as-yet unexplained low energy excess of electromagnetic activity observed by the MiniBooNE Collaboration [34].

Over the past decade, there has been a rich and evolving landscape of theoretical interpretations to explain the origin of the observed MiniBooNE excess, including standard processes [35] as well as new physics involving sterile neutrinos [36,37], dark sector portals [38–40], heavy neutral leptons [41,42], nonstandard Higgs physics [43–46], new particles produced in the beam [47,48], and mixed models of sterile neutrino oscillations and decay [49,50]. A number of scenarios have also been ruled

Published by the American Physical Society under the terms of the Creative Commons Attribution 4.0 International license. Further distribution of this work must maintain attribution to the author(s) and the published article's title, journal citation, and DOI. Funded by SCOAP³. out [51]. Because of the variety of theoretical explanations and their possible signatures, MicroBooNE has developed three distinct ν_e searches targeting the MiniBooNE signal: an exclusive search for two-body ν_e charged current quasielastic (CCQE) scattering, a semi-inclusive search for pionless ν_e events, and an inclusive ν_e search containing any hadronic final state. Additionally, a companion single-photon-based search focused on radiative decays of the Δ resonance is reported elsewhere [52]. This work capitalizes on the broad capabilities of a LArTPC to perform high purity measurements of electron neutrinos across multiple signal topologies and with significantly improved ability to distinguish whether an electromagnetic shower is electron or photon-induced compared to Cherenkov-based detectors such as MiniBooNE.

The advantage of this particular probe of the MiniBooNE signal is that MicroBooNE is located in the same neutrino beamline and at roughly the same location as MiniBooNE, but uses an imaging detector capable of mm-scale spatial resolution and substantially lower energy detection thresholds for many particle types. The MicroBooNE LArTPC [53,54] itself contains 85 tons of liquid argon and is sited 72.5 m upstream of the MiniBooNE detector hall at a distance of 468.5 m from the BNB proton target.

The data used in this work are taken from an exposure of 7×10^{20} protons on target (POT) collected in neutrino mode, a 93.7% ν_{μ} (5.8% $\bar{\nu}_{\mu}$) pure beam, from February 2016 to July 2018. These results represent an initial probe

into electron neutrino production in the BNB using roughly half of the total data collected by MicroBooNE. Two different data streams are used in this analysis: an on-beam data sample triggered by BNB neutrino spills and an off-beam data sample taken during periods when no beam was received. The off-beam data sample is used for a direct data-based measurement of cosmic-induced backgrounds which are of importance given MicroBooNE's location near the surface.

While probing different event topologies with distinct event reconstruction methods, the three independent electron neutrino searches in MicroBooNE share several aspects in common. To simulate neutrino interactions in argon, the analyses rely on a GEANT4-based [55] simulation of the neutrino beam [56], a variation of the GENIE V3 event generator [57] specifically tuned to data that reflects our best knowledge of neutrino scattering in the BNB energy range [58], and a GEANT4-based [55] detector simulation for particle propagation, with the processing of the charge response of the TPC and modeling of scintillation light implemented in the LArSoft framework [59]. The data-driven detector simulation represents a significant upgrade from what has been historically available to model LArTPCs and incorporates pioneering work performed by MicroBooNE on wire signal processing [28,29], noise removal [31], electric field mapping [25,26], and detector calibrations [27].

A common framework is additionally used to evaluate neutrino flux, neutrino cross section, and detector systematics. The evaluation of neutrino flux uncertainties is built on techniques developed by MiniBooNE [56]. A total of more than 50 model parameters are varied within GENIE to assess uncertainties related to simulating neutrino interactions and final state effects in argon [58]. A full complement of LArTPC detector systematics are modeled, many with a novel data-driven technique built on comparisons of wire response in data and simulation [60]. In addition, beam-related ν_e event predictions and uncertainties are further constrained through calculation of conditional means and variances using data-driven measurements of neutrino charged current (CC) and neutral current (NC) interactions in MicroBooNE, with constraint samples tailored to each of the ν_e analysis approaches. Table I summarizes the signal definitions, constraint samples, and reconstruction approaches for the different analyses.

Common approaches are also used for assessing agreement between observed and predicted ν_e samples and for hypothesis testing related to the presence or absence of an anomalous ν_e rate. In each search, the neutrino energy (E_{ν}) is based on reconstructed final state particle energies [61–63]. Binned reconstructed E_{ν} distributions for data and simulation are then compared using a combined Neyman-Pearson test statistic, $\chi^2_{\rm CNP}$ [64], which approximates well to the Poisson-likelihood test statistic for low event numbers. Similar statistical studies are performed to test a model of the ν_e event excess with an E_{ν} spectrum

TABLE I. Summary of signal definitions, signal-constraining datasets, and reconstruction approaches used for each of the three MicroBooNE ν_e searches. All samples require fully contained events with the exception of the 1eX analysis which additionally uses both partially and fully contained ν_μ CC samples as constraints.

ν_e Final state	Signal constraints	Reconstruction approach
$ \begin{array}{c} 1e1p(0\pi) \text{ CCQE} \\ 1eN(\geq 1)p0\pi, \\ 1e0p0\pi \end{array} $	$ u_{\mu} \ \text{CCQE} $ $ u_{\mu} \ \text{CC}$	Deep learning [61] PANDORA [62]
1eX	$ u_{\mu} \text{ CC}, \nu_{\mu} \text{ CC } \pi^{0}, $ $ \nu_{\mu} \text{ NC } \pi^{0}$	Wire-Cell [63]

and normalization representative of that observed in the MiniBooNE experiment.

A blind analysis scheme was adopted in which the signal region BNB ν_e data were only accessed after each analysis was completed. Details on each ν_e analysis, including the optimization of purity and efficiency in each approach, databased sidebands and simulated datasets used to validate the analyses, as well as data and Monte Carlo comparisons in a variety of kinematics, can be found in Refs. [61–63]. The next three sections describe the strategy behind each of the ν_e searches and a summary of their results.

Two-body ν_e CCQE scattering (1e1p).—An exclusive selection of ν_e candidates satisfying two-body CCQE kinematic constraints is performed in MicroBooNE with an analysis strategy focused around the use of deeplearning techniques [61]. The CCQE process is predicted to dominate at low energies, with 77% of ν_e events below 500 MeV (in true E_{ν}) expected to interact via this channel in MicroBooNE. A strength of this selection is its clean final state topology, which simplifies event reconstruction and selection. The pure CCQE requirement also allows the use of kinematic variables for signal selection, such as proton momentum, transverse momentum, neutrino direction, momentum transfer, and Bjorken x. For this analysis, only fully contained candidate ν_e and ν_u interactions with one reconstructed final state lepton and proton are selected. Final-state particle content and kinematics are reconstructed by applying a combination of conventional and deep-learning tools to prepared event images. Conventional tools are used to remove cosmic backgrounds [15], identify candidate neutrino interaction vertices [65], and reconstruct final-state particle candidates and their kinematics [65,66], while convolutional neural networks (CNNs) are used to differentiate tracklike from showerlike image pixels [67] and determine particle species contained in event images [68]. After basic data quality selection criteria, boosted decision tree (BDT) ensembles exploit 23 (16) kinematic and topological variables, including those described above, to collect a purified CCQE ν_e (ν_μ) event set. The CNN

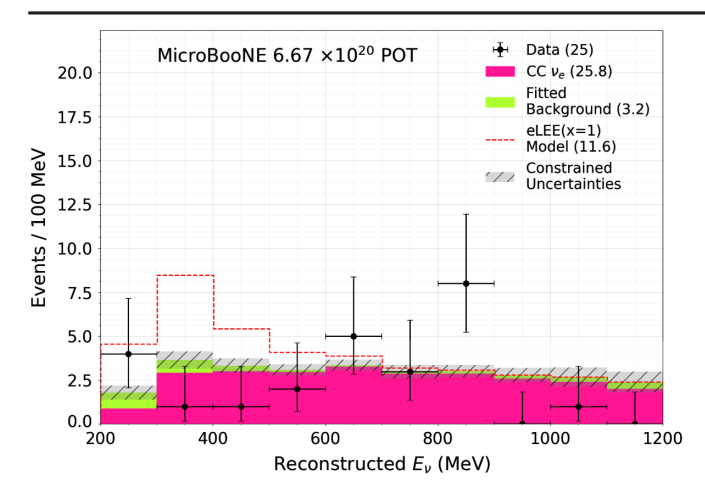


FIG. 1. Reconstructed neutrino energy for 1e1p CCQE candidate events in the deep-learning-based analysis. Backgrounds include contributions from cosmics and ν_{μ} interactions. The ν_{e} prediction constrained using ν_{μ} data is shown without (solid histogram) and with (red dotted) a model of the MiniBooNE low energy excess included (further detail in text). Systematic uncertainties on the constrained prediction are shown as a hatched band.

designed for particle identification is then used to select final candidates from this set.

The results of the ν_e CCQE analysis are shown in Fig. 1. This selection is predicted to produce a 75% (75%) pure sample of ν_e (ν_μ) CCQE events in the reconstructed E_ν range between 200 and 1200 MeV, with an efficiency of 6.6% for all true ν_e CCQE interactions in the LArTPC active volume. The average E_{ν} energy resolution for selected ν_e events is estimated to be 16.5%, with negligible bias predicted between true and reconstructed E_{ν} . The ν_e CCQE prediction is constrained using a high-statistics ν_{μ} CCQE candidate dataset, which increases predicted ν_{e} counts by 6% and reduces systematic uncertainties on the prediction by a factor of 2.0. Statistical uncertainties dominate the final measurement. The postconstraint prediction yields $29.0 \pm 5.2 (\text{stat}) \pm 1.9 (\text{syst})$ events in the full E_{ν} range given above (statistical errors follow the CNP formalism [64]), with most events (89%) predicted to arise from CCQE and non-CCQE ν_e interactions intrinsic to the beam. In the final selection, a total of 25 data candidates are observed in this range. The $\chi^2_{\rm CNP}$ test statistic calculated between predicted and observed distributions is found to be 25.3 for the analysis in ten E_{ν} bins (where 6.9 units of $\chi^2_{\rm CNP}$ result from a single bin at 850 MeV), leading to a p value of 0.014. Below 500 MeV, the χ^2_{CNP} contribution is 7.9 for three E_{ν} bins, with data in two of the three bins falling slightly below predicted values.

Pionless ν_e scattering $(1eNp0\pi, 1e0p0\pi)$.—A higher statistics search for pionless ν_e interactions that includes any number of protons in the final state uses the PANDORA event reconstruction package [22], which has been

exercised over the years to produce a wide variety of MicroBooNE physics measurements [2–7,10,11]. The PANDORA pattern recognition software, which reconstructs and classifies LArTPC events, is combined with specialized tools that further remove cosmic-ray background events as well as identify the different particles produced in a neutrino interaction [69] and reconstruct their energies [6]. This search focuses on two exclusive channels with one electron and no pions in the final state: one with at least one visible proton $(1eNp0\pi, N \ge 1)$ and one with no visible protons $(1e0p0\pi)$. A strength of this selection is that the two topologies combined exactly replicate the electronlike signal event signature in MiniBooNE. This selection on fully contained events spanning neutrino energies from 10 to 2390 MeV provides an efficiency of 15% (9%) with a purity of 80% (43%) for $1eNp0\pi$ ($1e0p0\pi$) events. The typical energy resolution is 2% for protons, 3% for muons, and approximately 12% for electrons, resulting in a predicted E_{ν} resolution of 15% with ~5% bias. To constrain neutrino flux and cross section uncertainties on the predicted intrinsic ν_e event rate, this analysis uses a highstatistics, 77% pure ν_{μ} CC inclusive event sample [62] and makes use of the cosmic-ray tagger detector system in MicroBooNE [54] to further reduce cosmic backgrounds. This constraint reduces the systematic uncertainties in the ν_e selections by a factor of 1.7 and the result remains dominated by statistical uncertainties. This analysis is also validated using MicroBooNE data from the NuMI beam [70] that provides a large number of ν_e -argon interactions at a similar energy range as the BNB.

The results of the PANDORA-based pionless ν_e analysis are shown in Fig. 2. For the $1eNp0\pi$ channel, 64 ν_e data events are observed compared to $86.8 \pm 8.8 (\text{stat}) \pm$ 11.5(syst) events expected (statistical errors follow the CNP formalism), in a reconstructed E_{ν} range between 10 and 2390 MeV. For the $1e0p0\pi$ channel, 34 ν_e data events are observed compared to $30.2 \pm 5.6 (\text{stat}) \pm 4.3 (\text{syst})$ events expected over that same energy range. The data are consistent with the prediction: in the region 150 MeV $\leq E_{\nu} \leq$ 1550 MeV where the final statistical tests are performed, the $\chi^2_{\rm CNP}/ndf$ (and associated p relative to the nominal prediction are 14.9/10(0.194), 16.7.9/10(0.116), and 31.56/20(0.097)for the $1eNp0\pi$ channel, $1e0p0\pi$ channel, and both combined, respectively. As with the 1e1p CCQE search results, the data for the $1eNp0\pi$ channel fall slightly below prediction. For the $1e0p0\pi$ channel, the observed event count below 500 MeV is above prediction, albeit in a region with lower predicted ν_e purity.

Inclusive ν_e scattering (1eX).—The highest statistics ν_e analysis in MicroBooNE searches inclusively for all possible hadronic final states such as the type of analyses that will be performed in the future wide-band Deep Underground Neutrino Experiment (DUNE) which will have larger contributions from additional inelastic

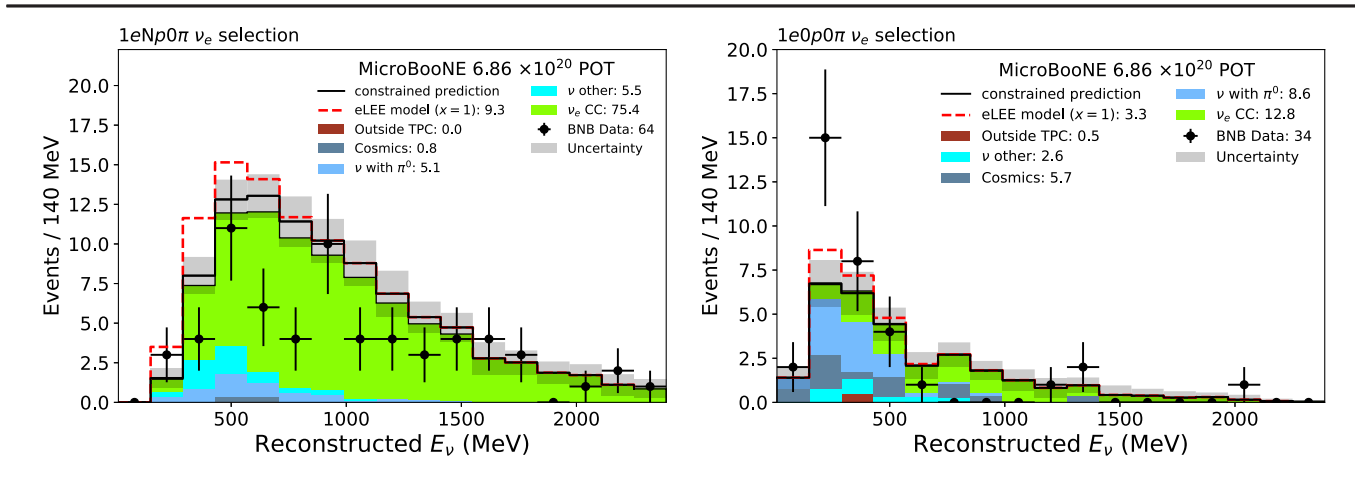


FIG. 2. Reconstructed neutrino energy for pionless ν_e candidate events in the PANDORA-based analysis: $1eNp0\pi$ (left) and $1e0p0\pi$ (right). Each of the plots extend from 10 to 2390 MeV with a 140 MeV bin width. The unconstrained number of predicted events is shown broken down by true interaction topology. The constrained predictions using ν_μ data are shown both with (red) and without (black) a model of the MiniBooNE low energy excess included (further detail in text). Systematic uncertainties on the constrained prediction are shown as a shaded band.

scattering processes at higher energies. This analysis uses the Wire-Cell reconstruction paradigm [71] which forms three-dimensional images of particle-induced electron ionization tracks and showers via 1D wire position tomography. The 3D images are then processed by clustering algorithms and matched to light signals for cosmic rejection [13,14,72], before a deep neural network [73] is used to determine the neutrino candidate vertex. Finally, the events are characterized in terms of energy deposit, topology, and kinematics, for eventual event building, classification (e.g., ν_e CC, ν_μ CC, π^0 , cosmic), and neutrino energy reconstruction. The strengths of this approach are its high efficiency and high purity. After all selections, the predicted efficiency for selecting inclusive ν_e CC (ν_μ CC) events is 46% (68%) with a purity of 82% (92%) for $0 < E_{\nu} <$ 2500 MeV. For fully contained events, the predicted calorimetric-based E_{ν} resolution is 10%–15% (15%–20%) for ν_e CC (ν_u CC) events with ~7% (10%) bias. In addition to the ν_{μ} CC data samples, which include both fully and partially contained events in the detector, CC and NC interactions with a reconstructed π^0 serve as additional constraints for reducing systematic uncertainties and therefore maximizing sensitivity. A high statistics sample of ν_e events from the NuMI beam also serves to validate the analysis. The constraints reduce the fractional uncertainty on the predicted number of fully contained ν_e CC events with reconstructed E_{ν} < 600 MeV by a factor of 3.5 relative to the unconstrained prediction. After constraints, the largest systematic uncertainties for fully contained ν_e CC events are associated with limited Monte Carlo statistics associated with this rare event search, detector effects (mainly recombination and wire response), and neutrino cross section modeling [58]. Compared to all systematic uncertainties, however, the statistical uncertainty on the data remains dominant.

Figure 3 shows the results of this inclusive ν_e search. The postconstraint ν_e CC inclusive analysis finds a modest deficit compared to the prediction: 56 (338) data events in $E_{\nu} < 600 \text{ MeV}$ ($0 < E_{\nu} < 2500 \text{ MeV}$) with $69.6 \pm 8.0 \text{(stat)} \pm 5.0 \text{(syst)}$ [384.9 \pm 19.2(stat) \pm 15.9(syst)] events expected. Good agreement is found between the data and the expectation from the BNB, with $\chi^2_{\text{Pearson}}/ndf = 17.9/25$ and a corresponding p value of 0.848, across all energies. Notably, agreement between the data and expectation is also apparent when the Wire-Cell inclusive event sample is studied in terms of its exclusive components, $1e0pX\pi$ and $1eNpX\pi$ ($X \ge 0$), where these subsamples are further described in Ref. [63].

Fit results.—The three aforementioned analysis selections are not designed to be disjoint to each other, and there is an overlap in the selected events. Of the 25 events selected in the 1e1p CCQE analysis, 16 are selected in either the pionless or inclusive analysis. Of the 98 events selected across both pionless analysis selections, 46 are selected in the inclusive analysis. All three analyses observe ν_e candidate event rates in general agreement with or below the predicted rates. Given the similar baseline and neutrino energies sampled by MicroBooNE and MiniBooNE, this picture appears to disfavor an interpretation of MiniBooNE's observed electronlike excess signature as arising purely from an anomalously high rate of charged current ν_e interactions. To more quantitatively address the comparison with the observed MiniBooNE data excess, all three analyses have performed statistical tests comparing datasets to a simple model of a MiniBooNE-like excess of ν_e interactions [74].

Using MiniBooNE simulation, a response matrix is constructed translating the true incident E_{ν} to reconstructed E_{ν} under a quasielastic assumption to the true incident E_{ν} , accounting for detector response, acceptance, resolutions,

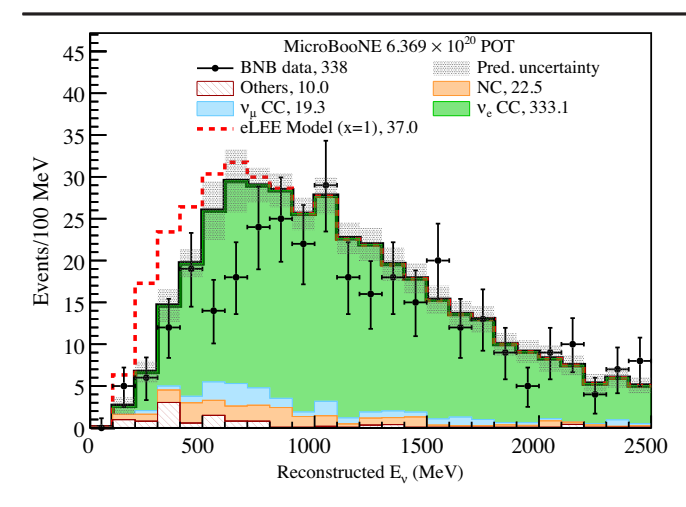


FIG. 3. Reconstructed neutrino energy for inclusive ν_e candidate events in the Wire-Cell based analysis. The predicted event sample is dominated by ν_e events intrinsic to the beam (green) while the other background contributions are described in the legend. The constrained predictions are shown both with (red) and without (black) a model of the MiniBooNE low energy excess included (further detail in text). Systematic uncertainties on the constrained prediction are shown as a shaded band.

event reconstruction, and selection efficiencies. Following a multidimensional unfolding procedure [75] on the MiniBooNE observation [76] and using only the statistical uncertainties on the MiniBooNE data and simulated events (to avoid any correlated uncertainties in flux and interaction

models with MicroBooNE), MicroBooNE extracts an energy-dependent event rate of ν_e interactions. The resulting scaling template, found to be robust against the number of unfolding iterations after an initial starting point corresponding to the MiniBooNE prediction, is derived from the increase in event rate relative to the MiniBooNE prediction and then applied to simulated intrinsic ν_e events in MicroBooNE to form an "eLEE" signal model, shown by the dashed lines in Figs. 1–3. This scaling template varies only in true neutrino energy, thus the electron Low Energy Excess (eLEE) model otherwise assumes the same kinematics and final-state topologies as MicroBooNE's ν_e simulation additional kinematic information from the MiniBooNE excess result is not considered. The range of the eLEE signal model is 200 < true E_{ν} < 800 MeV, as the unfolding procedure does not consider data below 200 MeV in neutrino energy and finds no significant excess at higher energies.

This simple model reproduces a median MiniBooNE electronlike excess to which MicroBooNE's results are compared, either by choosing a fixed excess normalization, x, matching MiniBooNE (x=1), or by treating x as a free parameter to be extracted. While the MiniBooNE uncertainties are not directly included in the eLEE model nor the statistical tests presented in this Letter, the reported significance of the excess from the MiniBooNE neutrinomode data [34], 4.69σ , translates to a 1σ confidence interval on the eLEE signal strength parameter of 1 ± 0.21 , illustrating how the MiniBooNE excess would appear. More rigorous comparisons of consistency with MiniBooNE in

TABLE II. Top: Observed and predicted ν_e candidates in the signal-enhanced neutrino energy range predefined by each analysis prior to unblinding, in the absence (x=0) or presence (x=1) of a MiniBooNE-like ν_e event excess. This energy range is a subset of the full fit range, also chosen prior to unblinding. Predicted events include the alternate-channel constraints of each analysis, and include statistical (following the CNP formalism) and constrained systematic uncertainties. Bottom: Frequentist-derived p values of the data observations compared to the prediction assuming no excess, $p(\chi^2_{x=0})$, and under a simple hypothesis test comparing an excess to no excess, $p(\Delta\chi^2 = \chi^2_{x=0} - \chi^2_{x=1} < \text{obs})$, assuming the eLEE model (x=1). Also quoted are the 1σ and 2σ confidence intervals for extracted signal strength x over the full fit range and the expected 2σ upper endpoint of the interval on x assuming no excess.

Signal-enhanced region comparison					
	1e1p CCQE	$1eNp0\pi$	$1e0p0\pi$	1eX	
E_{ν} (MeV)	200–500	150-650	150–650	0–600	
Predicted, no eLEE	8.8 ± 3.0	30.4 ± 6.1	19.0 ± 5.3	69.6 ± 9.4	
Predicted, w/eLEE	18.5 ± 4.4	39.0 ± 6.8	22.3 ± 5.7	104 ± 12	
Observed	6	21	27	56	
Final fit results					
	1e1p CCQE	$1eNp0\pi$	$1e0p0\pi$	1eX	
E_{ν} (MeV)	200-1200	150–1550	150–1550	0–2500	
$p(\chi^2_{r=0})$	1.4×10^{-2}	0.18	0.13	0.85	
$p(\Delta \chi^2 < \text{obs})$, w/eLEE	1.6×10^{-4}	2.1×10^{-2}	0.93	9.0×10^{-5}	
x observed, 1σ	[0.00, 0.08]	[0.00, 0.41]	[1.91,8.10]	[0.00, 0.22]	
x observed, 2σ	[0.00, 0.38]	[0.00, 1.06]	[0.77,24.3]	[0.00, 0.51]	
x expected upper limit, 2σ	0.98	1.44	4.64	0.56	

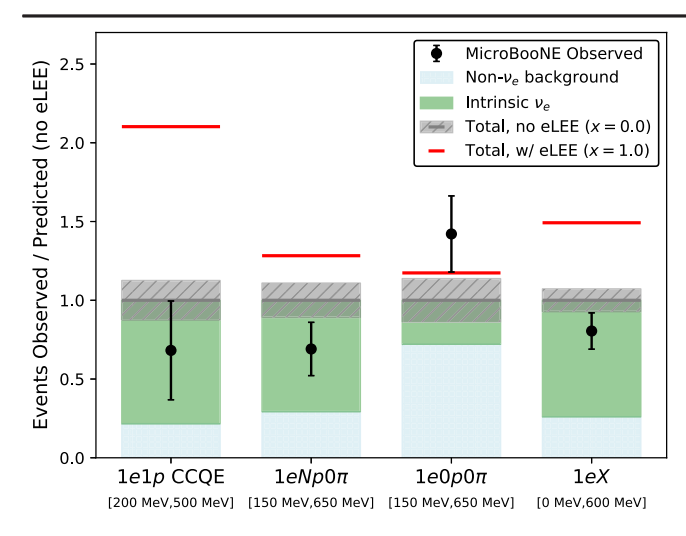


FIG. 4. Ratio of observed to predicted ν_e candidate events—assuming no eLEE—in each analysis's signal-enhanced neutrino energy range (see Table II, left) with the relative contributions shown from non- ν_e backgrounds (light blue) and intrinsic ν_e 's (green). Statistical errors are shown on the observations (black), while systematic errors are shown around the prediction (gray). The expected ratio assuming the MiniBooNE-like eLEE signal model with its median signal strength is also shown (red).

the future will need to consider correlated uncertainties in the neutrino flux and cross section models, as well as additional kinematic measurements.

Prior to unblinding of the data, each analysis defined a signal-enhanced low-energy region and determined the predicted number of events with and without the excess model in that region. Those predictions and the observed number of events are shown in Table II (top) and as ratios relative to the x=0 prediction in Fig. 4.

Each analysis performs two statistical analyses to test the signal hypothesis. First, a simple hypothesis test uses $\Delta\chi^2_{\rm CNP} = \chi^2_{x=0} - \chi^2_{x=1}$ as a test statistic, comparing the observations to a frequentist $\Delta\chi^2_{\rm CNP}$ distribution derived from model simulations assuming x=0 and x=1. The p values corresponding to $\Delta\chi^2_{\rm CNP}$ being less than the observed value assuming an eLEE (no eLEE) signal is 1.6×10^{-4} (0.02), 0.021 (0.29), 0.93 (0.98), and 9.0×10^{-5} (0.33) in the 1e1p CCQE, $1eNp0\pi$, $1e0p0\pi$, and 1eX selections, respectively. Each selection shows a strong preference for the absence of an electronlike MiniBooNE signal, with the exception of the $1e0p0\pi$ selection, driven by a data excess in the lowest energy bins, which also contain the highest contributions from non- ν_e backgrounds.

Second, each analysis performs a nested hypothesis test where the eLEE signal strength x is varied, with a lower bound constraint at x=0. Each analysis independently finds a best-fit signal strength, x_{\min} , by minimizing χ^2_{CNP} . Following this, a test statistic defined as $\Delta \chi^2(x) = \chi^2_{\text{CNP}}(x) - \chi^2_{\text{CNP}}(x_{\min})$ can be constructed for varying hypothetical signal strengths. A Feldman-Cousins method [77]

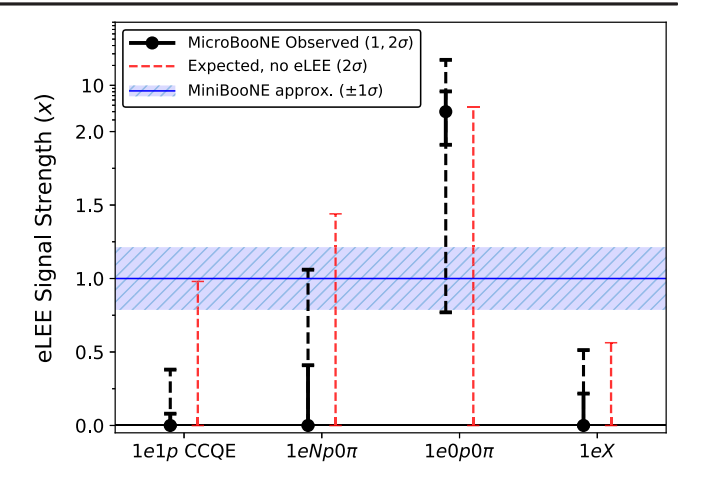


FIG. 5. Result of best-fit eLEE signal strength (x) in each analysis (black), along with the 1 and 2σ confidence intervals (solid and dashed lines, respectively). The expected 2σ upper bound for each analysis, assuming no eLEE signal, is also shown (red). Signal strength values approximated from the MiniBooNE statistical and systematic errors (at 1σ) are shown for comparison (blue). Note that the vertical scale is presented as linear from x = 0 to x = 2, while in logarithmic scale beyond that.

is used to construct confidence intervals around the best-fit signal strength, which are shown in Table II (bottom) and Fig. 5. Consistent with the observed deficit of events at low reconstructed energies, the 1e1p CCQE, $1eNp0\pi$, and 1eXselections each find a best fit signal strength of x = 0, corresponding to the absence of an observed event excess, with 2σ upper bounds at x < 0.38, < 1.06, and < 0.51, respectively. The expected 2σ upper bounds for these selections, assuming no signal, are shown in Table II. Consistent with the fact that in most analyses the observed number of events is less than the predicted number in the low energy regions, the measured upper endpoints of the 2σ interval are lower than expected. The best-fit signal strength for the $1e0p0\pi$ selection is x = 4.0, but with a wide confidence interval due to the low sensitivity of this channel. The best-fit signal strength for the $1eNp0\pi$ and $1e0p0\pi$ channels combined is x = 0.36, with x < 1.86at the 2σ confidence level (and an expected upper bound where there is no signal at x < 1.37), with more details in [62].

Conclusions.—The MicroBooNE experiment has performed a set of inclusive and exclusive searches for ν_e CC events using 7×10^{20} POT of Fermilab BNB neutrinomode data, about half of the collected dataset, with each analysis considering a hypothesis for the nature of the MiniBooNE low-energy excess. This work and Ref. [52] represent the first detailed study of this excess, noting that future MicroBooNE and short-baseline neutrino [78] measurements will continue to scrutinize the MiniBooNE results. The independent MicroBooNE search approaches have been led by distinct groups with each using a different fully automated event reconstruction software and common

data-blindness scheme. All results reported here are unchanged since data unblinding.

Afforded by the capabilities of the LArTPC technology to image various leptonic and hadronic final states, the searches all feature excellent signal identification and background rejection. In addition, the analyses use data-driven ν_e estimates constrained by high-statistics samples of π^0 and ν_μ CC events. The expected event rate is dominated by intrinsic ν_e CC events originating from the beamline, rather than background events involving photons. Despite the near-surface location, cosmic rays represent a subdominant and usually negligible contribution to the backgrounds.

No excess of low-energy ν_e candidates is observed, and the mutually compatible, statistics-limited measurements are either consistent with or modestly lower than the predictions for all ν_e event classes, including inclusive and exclusive hadronic final states, and across all energies. With the exception of the $1e0p0\pi$ selection which is the least sensitive to a simple model of the MiniBooNE lowenergy excess, MicroBooNE rejects the hypothesis that ν_e CC interactions are fully responsible for that excess (x = 1)at > 97% CL for both exclusive (1e1p CCQE, 1eNp0 π) and inclusive (1eX) event classes. Additionally, MicroBooNE disfavors generic ν_e interactions as the primary contributor to the excess, with a 1σ (2σ) upper limit on the inclusive ν_e CC contribution to the excess of 22% (51%). While the MiniBooNE excess remains unexplained, our sensitive measurements are so far inconsistent with a ν_e interpretation of the excess.

This document was prepared by the MicroBooNE Collaboration using the resources of the Fermi National Accelerator Laboratory (Fermilab), a U.S. Department of Energy, Office of Science, HEP User Facility. Fermilab is managed by Fermi Research Alliance, LLC (FRA), acting under Contract No. DE-AC02-07CH11359. MicroBooNE is supported by the following: the U.S. Department of Energy, Office of Science, Offices of High Energy Physics and Nuclear Physics; the U.S. National Science Foundation; the Swiss National Science Foundation; the Science and Technology Facilities Council (STFC), part of the United Kingdom Research and Innovation; the Royal Society (United Kingdom); and The European Unions Horizon 2020 Marie Sklodowska-Curie Actions. Additional support for the laser calibration system and cosmic-ray tagger was provided by the Albert Einstein Center for Fundamental Physics, Bern, Switzerland. We also acknowledge the contributions of technical and scientific staff to the design, construction, and operation of the MicroBooNE detector as well as the contributions of past collaborators to the development of MicroBooNE analyses, without whom this work would not have been possible.

- *microboone_info@fnal.gov
- [1] P. Abratenko *et al.* (MicroBooNE Collaboration), Phys. Rev. Lett. **128**, 151801 (2022).
- [2] P. Abratenko *et al.* (MicroBooNE Collaboration), Phys. Rev. D **104**, 052002 (2021).
- [3] P. Abratenko *et al.* (MicroBooNE Collaboration), Phys. Rev. D **102**, 112013 (2020).
- [4] P. Abratenko *et al.* (MicroBooNE Collaboration), Phys. Rev. Lett. **125**, 201803 (2020).
- [5] P. Abratenko *et al.* (MicroBooNE Collaboration), Phys. Rev. Lett. **123**, 131801 (2019).
- [6] C. Adams *et al.* (MicroBooNE Collaboration), Phys. Rev. D 99, 091102 (2019).
- [7] C. Adams *et al.* (MicroBooNE Collaboration), Eur. Phys. J. C 79, 248 (2019).
- [8] P. Abratenko *et al.* (MicroBooNE Collaboration), J. Instrum. **16**, P04004 (2021).
- [9] P. Abratenko *et al.* (MicroBooNE Collaboration), J. Instrum. **16**, P02008 (2021).
- [10] P. Abratenko *et al.* (MicroBooNE Collaboration), Phys. Rev. Lett. **127**, 151803 (2021).
- [11] P. Abratenko *et al.* (MicroBooNE Collaboration), Phys. Rev. D **101**, 052001 (2020).
- [12] P. Abratenko *et al.* (MicroBooNE Collaboration), arXiv: 2109.02460.
- [13] P. Abratenko *et al.* (MicroBooNE Collaboration), Phys. Rev. Applied **15**, 064071 (2021).
- [14] P. Abratenko *et al.* (MicroBooNE Collaboration), arXiv: 2012.07928.
- [15] P. Abratenko *et al.* (MicroBooNE Collaboration), J. Instrum. 16, P06043 (2021).
- [16] P. Abratenko *et al.* (MicroBooNE Collaboration), Phys. Rev. D **103**, 052012 (2021).
- [17] P. Abratenko *et al.* (MicroBooNE Collaboration), Phys. Rev. D **103**, 092003 (2021).
- [18] P. Abratenko *et al.* (MicroBooNE Collaboration), J. Instrum. 16, P02017 (2021).
- [19] C. Adams *et al.* (MicroBooNE Collaboration), J. Instrum. **15**, P02007 (2020).
- [20] C. Adams *et al.* (MicroBooNE Collaboration), Eur. Phys. J. C **79**, 673 (2019).
- [21] C. Adams *et al.* (MicroBooNE Collaboration), Phys. Rev. D 99, 092001 (2019).
- [22] R. Acciarri et al. (MicroBooNE Collaboration), Eur. Phys. J. C 78, 82 (2018).
- [23] R. Acciarri *et al.* (MicroBooNE Collaboration), J. Instrum. **12**, P03011 (2017).
- [24] P. Abratenko *et al.* (MicroBooNE Collaboration), J. Instrum. **16**, P09025 (2021).
- [25] P. Abratenko *et al.* (MicroBooNE Collaboration), J. Instrum. **15**, P12037 (2020).
- [26] C. Adams *et al.* (MicroBooNE Collaboration), J. Instrum. **15**, P07010 (2020).
- [27] C. Adams *et al.* (MicroBooNE Collaboration), J. Instrum. 15, P03022 (2020).
- [28] C. Adams *et al.* (MicroBooNE Collaboration), J. Instrum. 13, P07006 (2018).
- [29] C. Adams *et al.* (MicroBooNE Collaboration), J. Instrum. **13**, P07007 (2018).

- [30] R. Acciarri et al. (MicroBooNE Collaboration), J. Instrum. 12, P12030 (2017).
- [31] R. Acciarri et al. (MicroBooNE Collaboration), J. Instrum. 12, P08003 (2017).
- [32] R. Acciarri *et al.* (MicroBooNE Collaboration), J. Instrum. **12**, P09014 (2017).
- [33] P. Abratenko et al. (MicroBooNE Collaboration), J. Instrum. 12, P10010 (2017).
- [34] A. A. Aguilar-Arevalo *et al.* (MiniBooNE Collaboration), Phys. Rev. D **103**, 052002 (2021).
- [35] C. Giunti, A. Ioannisian, and G. Ranucci, J. High Energy Phys. 11 (2020) 146; 02 (2021) 078(E).
- [36] K. N. Abazajian et al., arXiv:1204.5379.
- [37] Y. Bai, R. Lu, S. Lu, J. Salvado, and B. A. Stefanek, Phys. Rev. D 93, 073004 (2016).
- [38] E. Bertuzzo, S. Jana, P. A. N. Machado, and R. Zukanovich Funchal, Phys. Rev. Lett. 121, 241801 (2018).
- [39] A. Abdullahi, M. Hostert, and S. Pascoli, Phys. Lett. B 820, 136531 (2021).
- [40] L. Alvarez-Ruso and E. Saul-Sala, in Prospects in Neutrino Physics (2017), arXiv:1705.00353.
- [41] P. Ballett, S. Pascoli, and M. Ross-Lonergan, Phys. Rev. D 99, 071701(R) (2019).
- [42] S. N. Gninenko, Phys. Rev. D 83, 093010 (2011).
- [43] B. Dutta, S. Ghosh, and T. Li, Phys. Rev. D 102, 055017 (2020).
- [44] J. Asaadi, E. Church, R. Guenette, B. J. P. Jones, and A. M. Szelc, Phys. Rev. D 97, 075021 (2018).
- [45] W. Abdallah, R. Gandhi, and S. Roy, Phys. Rev. D 104, 055028 (2021).
- [46] W. Abdallah, R. Gandhi, and S. Roy, J. High Energy Phys. 12 (2020) 188.
- [47] C.-H. V. Chang, C.-R. Chen, S.-Y. Ho, and S.-Y. Tseng, Phys. Rev. D 104, 015030 (2021).
- [48] V. Brdar, O. Fischer, and A. Y. Smirnov, Phys. Rev. D 103, 075008 (2021).
- [49] S. Vergani, N. W. Kamp, A. Diaz, C. A. Argüelles, J. M. Conrad, M. H. Shaevitz, and M. A. Uchida, Phys. Rev. D 104, 095005 (2021).
- [50] O. Fischer, A. Hernández-Cabezudo, and T. Schwetz, Phys. Rev. D 101, 075045 (2020).
- [51] J. R. Jordan, Y. Kahn, G. Krnjaic, M. Moschella, and J. Spitz, Phys. Rev. Lett. 122, 081801 (2019).
- [52] P. Abratenko *et al.* (MicroBooNE Collaboration), Phys. Rev. Lett. **128**, 111801 (2022).
- [53] R. Acciarri *et al.* (MicroBooNE Collaboration), J. Instrum. **12**, P02017 (2017).
- [54] C. Adams *et al.* (MicroBooNE Collaboration), J. Instrum. 14, P04004 (2019).

- [55] S. Agostinelli et al. (GEANT4 Collaboration), Nucl. Instrum. Methods Phys. Res., Sect. A 506, 250 (2003).
- [56] A. A. Aguilar-Arevalo et al. (MiniBooNE Collaboration), Phys. Rev. D 79, 072002 (2009).
- [57] C. Andreopoulos *et al.*, Nucl. Instrum. Methods Phys. Res., Sect. A **614**, 87 (2010).
- [58] P. Abratenko *et al.* (MicroBooNE Collaboration), Phys. Rev. D **105**, 072001 (2022).
- [59] E. Church et al. (LArSoft Collaboration), https://larsoft.org, arXiv:1311.6774.
- [60] P. Abratenko *et al.* (MicroBooNE Collaboration), arXiv: 2111.03556.
- [61] P. Abratenko et al. (MicroBooNE Collaboration), companion paper, Phys. Rev. D 105, 112003 (2022).
- [62] P. Abratenko et al. (MicroBooNE Collaboration), companion paper, Phys. Rev. D 105, 112004 (2022).
- [63] P. Abratenko *et al.* (MicroBooNE Collaboration), companion paper, Phys. Rev. D 105, 112005 (2022).
- [64] X. Ji, W. Gu, X. Qian, H. Wei, and C. Zhang, Nucl. Instrum. Methods Phys. Res., Sect. A 961, 163677 (2020).
- [65] P. Abratenko *et al.* (MicroBooNE Collaboration), J. Instrum. 16, P02017 (2021).
- [66] P. Abratenko *et al.* (MicroBooNE Collaboration), J. Instrum. **16**, T12017 (2021).
- [67] P. Abratenko *et al.* (MicroBooNE Collaboration), Phys. Rev. D **103**, 052012 (2021).
- [68] P. Abratenko *et al.* (MicroBooNE Collaboration), Phys. Rev. D **103**, 092003 (2021).
- [69] P. Abratenko et al. (MicroBooNE Collaboration), J. High Energy Phys. 12 (2021) 153.
- [70] P. Adamson *et al.*, Nucl. Instrum. Methods Phys. Res., Sect. A **806**, 279 (2016).
- [71] X. Qian, C. Zhang, B. Viren, and M. Diwan, J. Instrum. 13, P05032 (2018).
- [72] P. Abratenko *et al.* (MicroBooNE Collaboration), J. Instrum. **16**, P06043 (2021).
- [73] P. Abratenko *et al.* (MicroBooNE Collaboration), J. Instrum. **17**, P01037 (2022).
- [74] P. Abratenko *et al.* (MicroBooNE Collaboration), https://microboone.fnal.gov/wp-content/uploads/MICROBOONE-NOTE-1043-PUB.pdf.
- [75] G. D'Agostini, Nucl. Instrum. Methods Phys. Res., Sect. A 362, 487 (1995).
- [76] A. A. Aguilar-Arevalo *et al.* (MiniBooNE Collaboration), Phys. Rev. Lett. **121**, 221801 (2018).
- [77] G.J. Feldman and R.D. Cousins, Phys. Rev. D **57**, 3873 (1998).
- [78] M. Antonello *et al.* (MicroBooNE, LAr1-ND, ICARUS-WA104 Collaborations), arXiv:1503.01520.